Tunable Band Structures of Heterostructured Bilayers with Transition-Metal Dichalcogenide and MXene Monolayer

ARTICLE *in* THE JOURNAL OF PHYSICAL CHEMISTRY C · MARCH 2014

Impact Factor: 4.77 · DOI: 10.1021/jp500861n

7 AUTHORS, INCLUDING:

Zhenpeng hu
Nankai University
39 PUBLICATIONS **771** CITATIONS
SEE PROFILE

Qing Tang
University of California, Riverside
41 PUBLICATIONS **763** CITATIONS
SEE PROFILE

Zhen Zhou
Nankai University
213 PUBLICATIONS **6,983** CITATIONS
SEE PROFILE

THE JOURNAL OF PHYSICAL CHEMISTRY C

Article

pubs.acs.org/JPCC

Tunable Band Structures of Heterostructured Bilayers with Transition-Metal Dichalcogenide and MXene Monolayer

Zhinan Ma, Zhenpeng Hu, Xudong Zhao, Qing Tang, Dihua Wu, Zhen Zhou,* and Lixin Zhang

Tianjin Key Laboratory of Metal and Molecule Based Material Chemistry, Key Laboratory of Advanced Energy Materials Chemistry (Ministry of Education), Computational Centre for Molecular Science, Institute of New Energy Material Chemistry, Collaborative Innovation Center of Chemical Science and Engineering (Tianjin), School of Physics, Nankai University, Tianjin 300071, P. R. China

Supporting Information

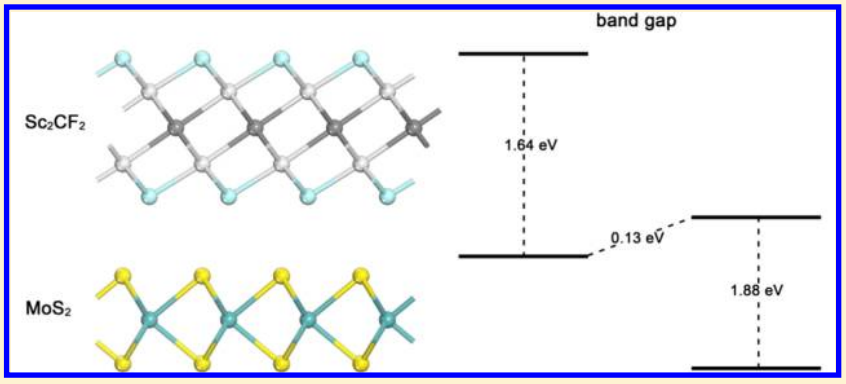

ABSTRACT: Forming bilayer or multilayer heterostructures via interlayer van der Waals interactions is a superior preparation strategy for two-dimensional heterojunctions. In this work, by employing density functional theory computations, we investigated heterostructured bilayers of transition-metal dichalcogenides (TMDs) (including MoS_2, WS_2, $MoSe_2$, and WSe_2) and MXene (exemplified by Sc_2CF_2) monolayer. All TMD and Sc_2CF_2 materials are hexagonal with little mismatch. Compared with separate TMD and Sc_2CF_2 monolayers, TMD−Sc_2CF_2 bilayers can be tuned to indirect semiconductors with the band gaps of 0.13−1.18 eV; more importantly, they are type-II heterostructures with the valence band maximum and conduction band minimum located at Sc_2CF_2 and TMDs, respectively. Stretching or compressing would reduce or enlarge the band gaps of the heterostructures, respectively. The tunable band structures make TMD−Sc_2CF_2 bilayers pomising candidates for electronic device applications.

INTRODUCTION

Since graphene was experimentally realized, more two-dimensional (2D) materials have emerged with unique physical and chemical properties.[1,2] For finely tuning the properties of 2D materials, versatile modifications have been applied, such as introduction of doping elements or defects, fabrication of heterojunctions, and functionalization with various groups. Forming heterojunctions is a very useful method;[3−5] however, the inevitable boundary state is usually dominant in the properties of heterostructures. Recently a new strategy for heterostructures has succeeded in experiments by layering one monolayer on top of another monolayer or a few-layer crystal as the substrate through van der Waals (vdW) interactions.[6−11] In experiments with different substrates, graphene exhibits superlattice Dirac points, improved on−off ratio, and a variety of nontrivial integer and fractional quantum Hall states.[8−11] In computations, vdW heterostructures exhibit robust structural and physical properties.[12−22] Therefore, exploring more multilayer vdW heterostructures with novel structures and superior properties is of great significance.

Transition-metal dichalcogenide (TMD) 2D semiconductors, such as MoS_2, WS_2, $MoSe_2$, and WSe_2, have been attracting great interest because of their graphene-like structure, direct band gap, and fast lithium diffusion. These properties make TMD 2D materials potential candidates for logic transistors, chemical sensors, and Li ion battery anodes.[23−31] TMD monolayers conjoining with other 2D materials have captured much attention for the superior properties.[9,11,18−20] For example, MoS_2 and WS_2 could form field-effect tunneling transistors with graphene.[9,11] Computationally, MoS_2 was found to open a band gap at the Dirac point of graphene.[15] When integrated with each other to form TMD−TMD bilayers, like MoS_2−WS_2, TMDs could form type-II heterostructured semiconductors.[18,19,21,22]

Recently, another star material, MXene, such as Ti_2CF_2 and $Ti_2C(OH)_2$, was integrated with MoS_2 computationally to form vdW heterostructured bilayers with *n*-type Schottky barrier height of 0.85 and 0.26 eV, respectively.[20] MXene is a new type of graphene-like materials prepared from layered MAX phases, where M represents Ti, Sr, V, Cr, Ta, Nb, Zr, Mo, or Hf, A

Received: January 24, 2014
Revised: February 19, 2014
Published: February 21, 2014

   dx.doi.org/10.1021/jp500861n | *J. Phys. Chem. C* 2014, 118, 5593−5599

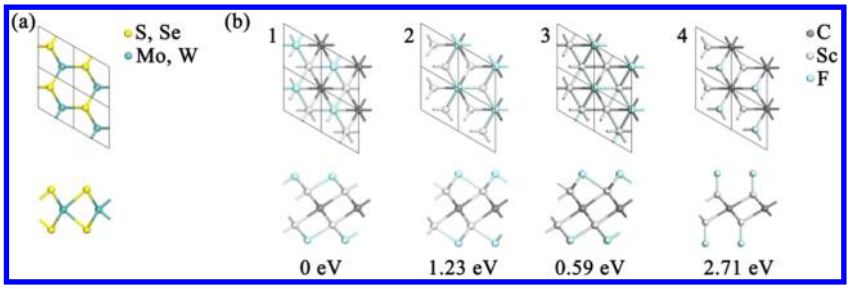

Figure 1. Top and side views of (a) TMD single layer and (b) four models of Sc_2CF_2 single layer in 2 × 2 supercells.

represents Al, Ga, In, Ti, Si, Ge, Sn, or Pb, and X represents C, N, or both.[32,33] In recent studies, MXenes have demonstrated versatile electronic properties and potential applications to energy storage.[34−37]

As two attractive materials, MXene and TMD are highly expected to generate more properties by forming heterojunction structures with each other. Very recently, vdW heterostructures composed of semiconducting TMD (MoS_2) and metallic MXene (Ti_2CF_2 and $Ti_2C(OH)_2$) have been investigated.[20] To investigate semiconductor−semiconductor heterostructures of TMD and MXene, we chose Sc_2CF_2, a semiconductor MXene, to form TMD−Sc_2CF_2 bilayers, including MoS_2−Sc_2CF_2, WS_2−Sc_2CF_2, $MoSe_2$−Sc_2CF_2, and WSe_2−Sc_2CF_2, for density functional theory (DFT) computations.[34] As two semiconductoring TMD monolayers could form type-II heterostructured bilayers,[18,19] Sc_2CF_2 monolayer, with a band gap (1.03 eV[34]) similar to those of TMD monolayers (1.55−1.99 eV), are expected to form type-II heterostructured bilayers.[23,25,26,38] In particular, layered Sc_2CCl_2 bulk crystal, a Sc_2CF_2 analogue, has been prepared experimentally, which implies that a Sc_2CF_2 layer is feasible for synthesis.[39]

In this work, first we optimized the geometries of the monolayer materials (MoS_2, WS_2, $MoSe_2$, WSe_2, and Sc_2CF_2) and then checked the stability of the Sc_2CF_2 2D structure through a phonon dispersion spectrum. Then we computed the band structures of monolayers and bilayer heterostrcutures and checked the spatial distribution of the valence band maximum (VBM) and conduction band minimum (CBM) for these heterostructures. Finally, we computed the band gaps of stretched and compressed heterostructures.

COMPUTATIONAL DETAILS

Our DFT computations were performed with plane-wave pseudopotentials implemented in CASTEP code.[40] The generalized gradient approximation (GGA) for exchange-correlation term was employed, and the PW91 functional was adopted for structure optimization.[41] To acquire accurate results for bilayer structures, DFT-D approach was included with the Ortmann−Bechstedt−Schmidt (OBS) vdW correction.[42] The cutoff energy was set as 400 eV, and self-consistent field (SCF) computations were adopted with a convergence of 10^{-6} eV/atom. For band structure computations, besides PW91, the hybrid functional of Heyd−Scuseria−Ernzerhof (HSE) was also used for better description.[43] For PW91 computations, 6 × 6 × 1 k-points were used for sampling the Brillouin zone; however, because of the huge computational consumption of HSE, the mesh of 4 × 4 × 1 was used for band structures and 7 × 7 × 1 for density of states (DOS). For the computation of the phonon dispersion spectrum of Sc_2CF_2 by PW91 with density functional perturbation theory (DFPT), the cutoff energy was chosen as 480 eV and the mesh of 6 × 6 × 1 was used. All the computations were performed in supercells with a vacuum space larger than 10 Å above and below the layered materials.

RESULTS AND DISCUSSION

First we optimized the structures of TMD monolayers, MoS_2, WS_2, $MoSe_2$, and WSe_2. As a sandwich layer, two S (Se) atoms are located on both sides of Mo (W) atoms in the middle (Figure 1a). The S (Se) atoms on both sides point to each other through the hollow sites among three neighboring Mo (W) atoms.

Next, we optimized four configurations for Sc_2CF_2 single layer to find the lowest energy structure.[34] As shown in Figure 1b, all the models of Sc_2CF_2 are hexagonal layers. For model 1, all the F atoms are located above the hollow sites among three neighboring C atoms. In model 2, all F atoms point directly toward C atoms. Model 3 is a hybrid structure of model 1 and model 2 as half of F atoms on one side are located above the hollow sites of three neighboring C atoms and the remaining F atoms point toward the C atoms on the other side. For model 4, all F atoms are located on top of Sc atoms. In our computations model 1 is the most stable structure with the lowest energy and lattice parameters as $a = b = 3.28$ Å. For four models the energies relative to model 1 are also shown in Figure 1b. Model 3 is the second lowest energy structure with the energy of 0.59 eV larger than that of model 1. The largest-energy structure is model 4 with the fewest F−Sc bonds. These results are in agreement with a previous report.[34] We used model 1 in all the following computations as the structure of the Sc_2CF_2 layer.

In contrast to TMD monolayers, Sc_2CF_2 monolayer has not been prepared in experiments. Though the most stable structure (model 1) has been proposed for Sc_2CF_2 single layer, it is still necessary to confirm the stability of this configuration computationally. In Figure 2, the phonon dispersion spectrum was presented along the high-symmetry points in the Brillouin zone. There are no imaginary frequencies in the phonon dispersion spectrum, revealing that Sc_2CF_2 single layer is a stable structure and that it is possible to be realized in experiments. It is not surprising because model 1 is similar to layered Sc_2CCl_2, whose bulk crystal is available in experiments.[39]

TMD and Sc_2CF_2 layers are both hexagonal and are convenient for forming bilayer heterostructures in a hexagonal crystal theoretically. To obtain reasonable results in one cell for TMD−Sc_2CF_2 bilayers, low mismatch is necessary between TMDs and Sc_2CF_2. Table 1 shows all the lattice parameters of TMD and Sc_2CF_2 monolayers and the mismatches relative to Sc_2CF_2. In our computations, the mismatches are in the range of 0.9%∼2.8% and are low enough to ensure reliable results for vdW heterostructures. The band structures of TMDs and

dx.doi.org/10.1021/jp500861n | J. Phys. Chem. C 2014, 118, 5593−5599

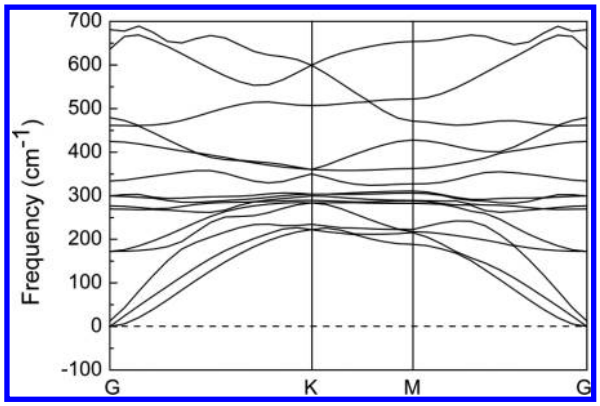

Figure 2. Phonon dispersion spectrum of Sc_2CF_2 single layer.

Table 1. Lattice Parameter (a), Mismatch Relative to Sc_2CF_2, and Band Gap of TMD and Sc_2CF_2 monolayers

monolayer		Sc_2CF_2	MoS_2	WS_2	$MoSe_2$	WSe_2
lattice parameter (a, Å)		3.28	3.19	3.19	3.31	3.31
mismatch (%)		0	2.8%	2.8%	0.9%	0.9%
band gap (eV)	PW91	1.05	1.62	1.77	1.43	1.51
	HSE	1.64	1.88	1.93	1.67	1.66
	experimental	–	1.90[23]	1.99[38]	1.55[25]	1.64[26]

Sc_2CF_2 were disclosed with PW91 and HSE computations (Figure 3 and Table 1). The band gap by PW91 for Sc_2CF_2 is 1.05 eV, which is similar to that given in a previous report.[34] In most cases PW91 underestimates the band gaps; therefore, a more accurate method, HSE, was also adopted here. As shown in Table 1, the results by HSE are closer to the experimental values than those by PW91.[23,25,26,38] The band gaps of TMD monolayers are in the range of 1.66−1.93 eV, larger than that of Sc_2CF_2 layer. The band structures are shown in Figure 3, and all the TMD monolayers are direct band gap semiconductors, in agreement with experiment results. The VBMs and CBMs of TMD monolayers are all at the K point of the Brillouin zone. In contrast to the TMD layers, Sc_2CF_2 monolayer has an indirect band gap with VBM and CBM at G and K points, respectively.

MoS_2−Sc_2CF_2, WS_2−Sc_2CF_2, $MoSe_2$−Sc_2CF_2, and WSe_2−Sc_2CF_2 bilayers were then optimized to investigate the structures and electronic properties. Though there are numerous patterns for TMD and Sc_2CF_2 stacking, only six high-symmetry patterns (A, B, C, D, E, and F in Figure 4) were considered here. Apparently in Sc_2CF_2, the F atoms are the closest to the TMD layers. For patterns A and B, the F atoms in

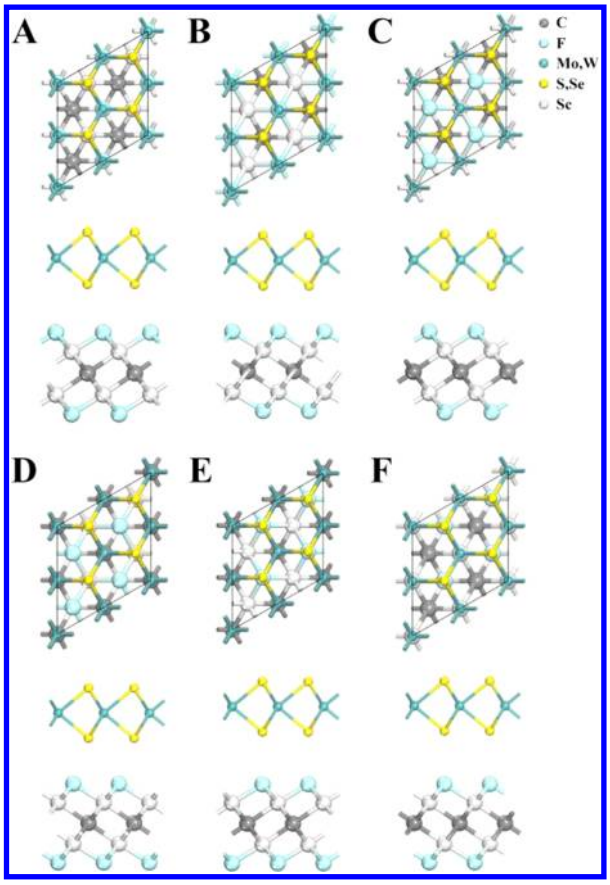

Figure 4. Six stacking patterns for TMD−Sc_2CF_2 bilayers with top (upper panels) and side (lower panels) views.

Sc_2CF_2 point to Mo (W) atoms in TMDs; for patterns C and D, the F atoms point to the hollows of TMDs; finally, for patterns E and F, the F atoms point to S (Se) atoms. For patterns A−D, one S (Se) in TMDs approaches three F atoms; in a similar way, F atoms approach three S (Se) atoms. In contrast to the stagger arrangement of S (Se) and F atoms in TMDs and Sc_2CF_2 in patterns A−D, the S atoms and F atoms point to each other in patterns E and F. To evaluate the vdW interactions between two layers, the distance D between S and F atoms and the binding energy ΔE were calculated for these heterostructrures:

$$\Delta E = E_{\text{heterostructure}} - E_{\text{TMD}} - E_{\text{Sc}_2\text{CF}_2}$$

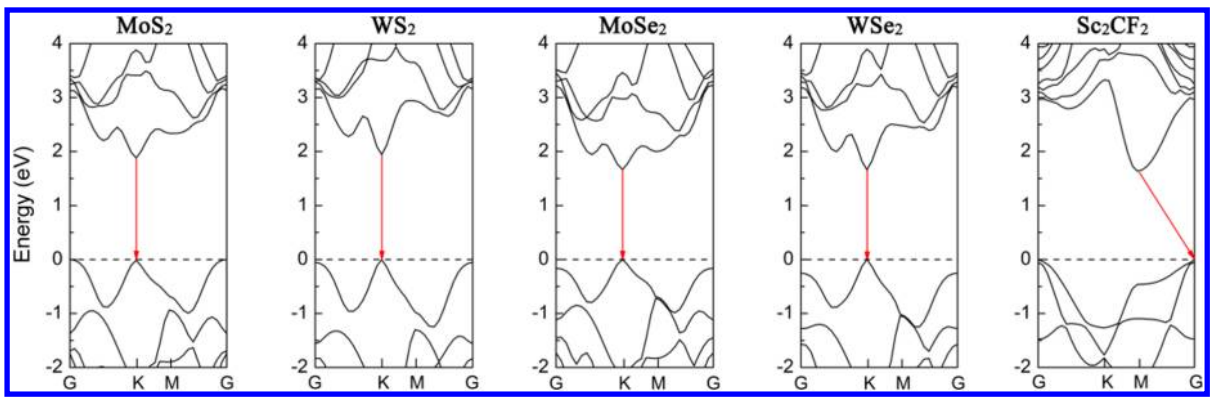

Figure 3. Band structures of TMD and Sc_2CF_2 monolayers by HSE. The VBM is regulated at 0 eV.

dx.doi.org/10.1021/jp500861n | J. Phys. Chem. C 2014, 118, 5593−5599

Table 2. Binding Energies (in Electronvolts) of Six Stacking Patterns for TMD−Sc_2CF_2 Bilayers

pattern	A	B	C	D	E	F
$\Delta E_{MoS_2-Sc_2CF_2}$ (eV)	−0.283	−0.279	−0.279	−0.282	−0.246	−0.245
$\Delta E_{WS_2-Sc_2CF_2}$ (eV)	−0.268	−0.264	−0.264	−0.268	−0.232	−0.231
$\Delta E_{MoSe_2-Sc_2CF_2}$ (eV)	−0.313	−0.296	−0.297	−0.308	−0.281	−0.271
$\Delta E_{WSe_2-Sc_2CF_2}$ (eV)	−0.307	−0.296	−0.292	−0.299	−0.261	−0.266

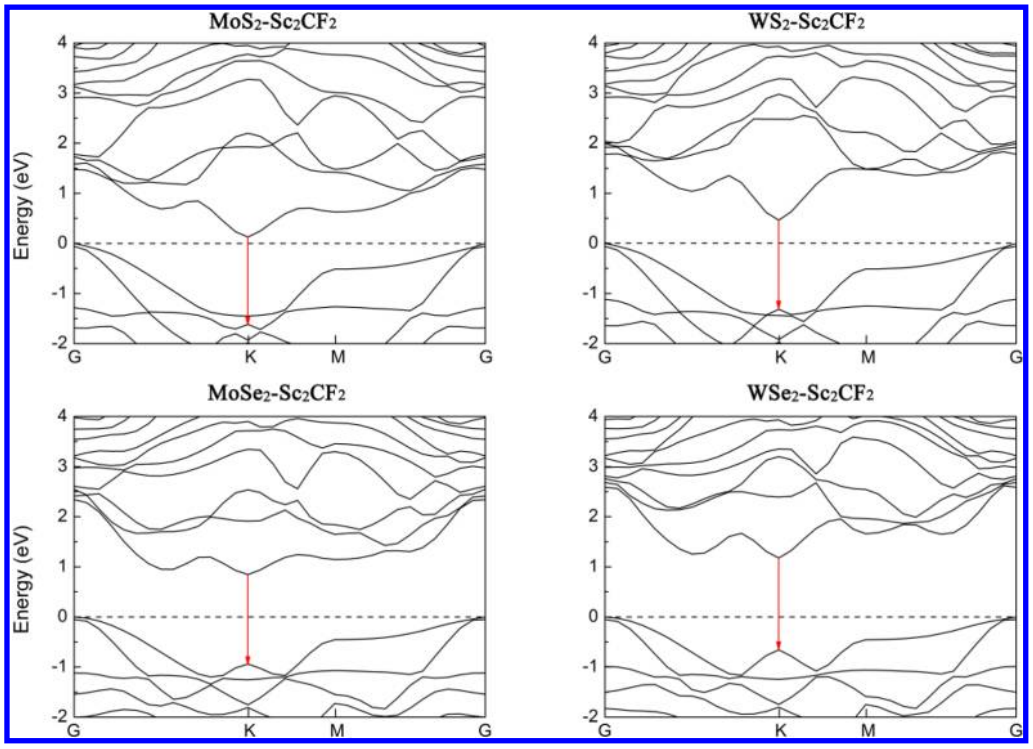

Figure 5. Band structures of TMD−Sc_2CF_2 bilayers by HSE. The VBM is regulated at 0 eV. Red arrows demonstrate direct band gaps of TMD.

where ΔE represents the binding energy for bilayers and $E_{heterostructure}$, E_{TMD}, and $E_{Sc_2CF_2}$ represent the total energy of heterostructrures, TMD, and Sc_2CF_2 monolayer, respectively. All the binding energies are in the range of 0.231−0.313 eV, which are in the range of physical adsorption. The distances between S (Se) and F atoms are approximately 3.3 Å, which means that no bonds form between S (Se) and F atoms. All these results support the vdW interaction between two layers. As shown in Table 2, because of different interaction areas, for all bilayers the binding energies of pattern A are larger than those of patterns B−F. Therefore, pattern A is the most stable structure and was used for the following computations.

Next, we investigated the band structures of various TMD−Sc_2CF_2 bilayers. The band structures of these bilayers are different from those of TMD and Sc_2CF_2 separate monolayers (Figure 5). The spin−orbit coupling (SOC) effect is significant on TMD monolayers, especially for WS_2 and WSe_2 monolayers;[18] however, the SOC effect has little impact on the band gaps of TMD−Sc_2CF_2 bilayers, and we could safely neglect the SOC effect in the computations (see detailed discussion in the Supporting Information). TMD monolayers are direct band gap semiconductors, while all these bilayers exhibit indirect band gaps, which would reduce the recombination of electron−hole pairs. The same as Sc_2CF_2 monolayer, the VBMs of TMD−Sc_2CF_2 bilayers are located at G point; however, the CBMs are located at K point, similar to TMD monolayers, demonstrating the formation of type-II band-offset semiconductors.

Because of the difference in band structures between the monolayers and bilayer vdW heterostructures, the changes of band gaps emerge in TMD−Sc_2CF_2 bilayers. The gap reductions of these bilayers are shown in Table 3. The largest gap reduction of 1.51 eV occurs to MoS_2−Sc_2CF_2. The lowest reduction is still up to 0.46 eV for WSe_2−Sc_2CF_2. As for MoS_2−WS_2 bilayers, the interlayer coupling is negligible; therefore, the band structures are determined by the superposition of the monolayer states.[18] While in TMD−Sc_2CF_2 bilayer systems, the band gaps could be tuned significantly, offering an opportunity for band structure engineering and

Table 3. Lattice Parameters (a) for Pattern A and Band Gaps for TMD−Sc_2CF_2 Bilayers[a]

bilayers	MoS_2−Sc_2CF_2	WS_2−Sc_2CF_2	$MoSe_2$−Sc_2CF_2	WSe_2−Sc_2CF_2
a (Å)	3.23	3.23	3.27	3.27
band gap (HSE) (eV)	0.13	0.46	0.86	1.18
gap reduction (eV)	1.51	1.18	0.78	0.46

[a]The band gaps for TMD−Sc_2CF_2 bilayers were computed on the basis of pattern A with HSE. The gap reduction represents the reduction of the band gaps for TMD−Sc_2CF_2 bilayers (pattern A) relative to Sc_2CF_2 monolayer.

dx.doi.org/10.1021/jp500861n | J. Phys. Chem. C 2014, 118, 5593−5599

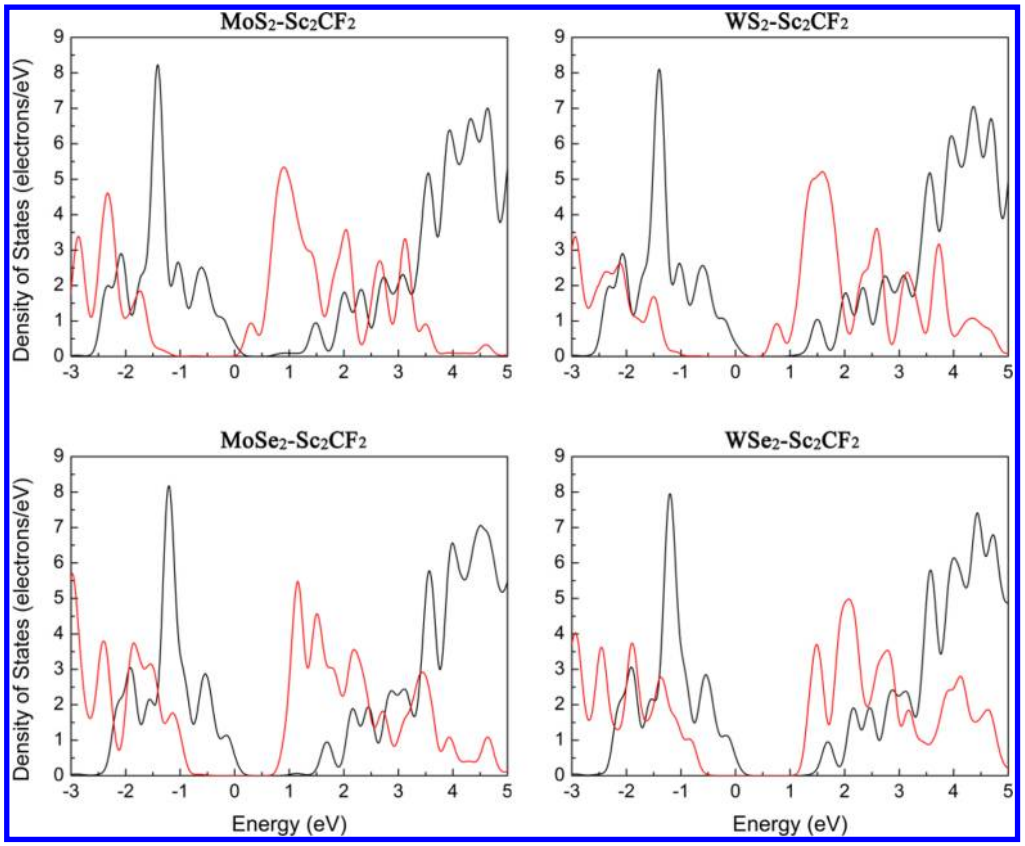

Figure 6. PDOSs for TMD−Sc_2CF_2 bilayers by HSE. Red and black lines represent the DOS of TMD and Sc_2CF_2 layer, respectively. The VBM is regulated at 0 eV.

electronic device design. To further clarify the electronic properties of TMD−Sc_2CF_2 bilayer heterostructure, we present the projected density of states (PDOS) in Figure 6. The black and red lines represent the DOS of TMD and Sc_2CF_2 in TMD−Sc_2CF_2 bilayers, respectively. It can be seen clearly that the VBMs and CBMs are confined in Sc_2CF_2 and TMDs, respectively, indicating that TMD−Sc_2CF_2 bilayers are type-II heterostructure semiconductors. Because the VBM and CBM for TMD−Sc_2CF_2 bilayers are located at Sc_2CF_2 and TMD monolayers, respectively, it is necessary to consider the excitonic effect for optical properties.[21] Therefore, we calculated the imaginary part of the dielectric constant (ε_2) for MoS_2−Sc_2CF_2 bilayer, MoS_2 monolayer, and Sc_2CF_2 monolayer as an example and found that the excitions are confined in each monolayer (Supporting Information).

Though the lattice mismatch of TMD−Sc_2CF_2 bilayers is small, both layers still have to be stretched or compressed to match each other. Therefore, it is necessary to investigate the band gaps of stretched or compressed bilayers. We optimized the structures and computed the band gaps of stretched/compressed TMD−Sc_2CF_2 bilayers with +1.5%/−1.5% lattice parameters larger/lower than those of TMD−Sc_2CF_2 bilayers investigated above. It can be seen from Tables 3 and 4 that stretching/compressing can result in the reduction/enlargement of band gaps for all bilayers. In particular, the +1.5% lattice turns stretched MoS_2−Sc_2CF_2 bilayer from a semiconductor into a metal. Accordingly, stretching/compressing offers a convenient way of tuning the band gaps of heterostructures.

Table 4. Lattice Parameters (a) for Pattern A, Binding Energies (ΔE), and Band Gaps for TMD−Sc_2CF_2 Bilayers

bilayer		MoS_2−Sc_2CF_2	WS_2−Sc_2CF_2	$MoSe_2$−Sc_2CF_2	WSe_2−Sc_2CF_2
stretched	a (Å)	3.27	3.28	3.32	3.32
	ΔE (eV)	−0.247	−0.226	−0.278	−0.260
	band gap (eV)	metallic	0.23	0.57	0.90
compressed	a (Å)	3.18	3.18	3.22	3.23
	ΔE	−0.249	−0.231	−0.278	−0.256
	band gap (eV)	0.45	0.80	0.89	1.20

CONCLUSION

In summary, by employing DFT computations, we have investigated the structural and electronic properties of TMD−Sc_2CF_2 bilayer vdW heterostructures. The phonon dispersion spectrum was computed to confirm the stability of Sc_2CF_2 monolayer. In agreement with experiments, all the TMD monolayers are direct band gap semiconductors with the band gaps of 1.66−1.93 eV. In contrast to TMD monolayers, Sc_2CF_2 monolayer is an indirect band gap (1.64 eV) semiconductor. Some high-symmetry stacking configurations were optimized for TMD−Sc_2CF_2 bilayer vdW structures, and the pattern of S atoms in MoS_2 pointing to the Sc atoms in Sc_2CF_2 is the most stable. With this stacking pattern, TMD−Sc_2CF_2 bilayers are changed into indirect band gap semiconductors with tunable gaps in the range of 0.13−1.18 eV, and more importantly, the VBMs and CBMs of TMD−Sc_2CF_2 bilayers are located at Sc_2CF_2 and TMDs, respectively, demonstrating type-II band offset. Stretching/compressing also offers a convenient way of

dx.doi.org/10.1021/jp500861n | J. Phys. Chem. C 2014, 118, 5593−5599

tuning the band gaps of the heterostructures. Tunable band structures and efficient electron−hole separation make TMD−Sc_2CF_2 vdW heterostructures promising candidates for electronic device applications.

■ ASSOCIATED CONTENT

Supporting Information

Computational details and results involving SOC or excitonic effect. This material is available free of charge via the Internet at http://pubs.acs.org.

■ AUTHOR INFORMATION

Corresponding Author

*E-mail: zhouzhen@nankai.edu.cn (ZZ).

Notes

The authors declare no competing financial interest.

■ ACKNOWLEDGMENTS

This work was supported by Tianjin Municipal Science and Technology Commission (12JCZDJC28100), NSFC (21273118), and MOE Innovation Team (IRT13022) in China. The computations were performed on Magic Cube at Shanghai Supercomputer Center.

■ REFERENCES

(1) Novoselov, K. S.; Geim, A. K.; Morozov, S. V.; Jiang, D.; Zhang, Y.; Dubonos, S. V.; Grigorieva, I. V.; Firsov, A. A. Electric Field Effect in Atomically Thin Carbon Films. *Science* **2004**, *306*, 666−669.

(2) Tang, Q.; Zhou, Z. Graphene-Analogous Low-Dimensional Materials. *Prog. Mater. Sci.* **2013**, *58*, 1244−1315.

(3) Watson, I. M. Metal Organic Vapour Phase Epitaxy of AlN, GaN, InN and Their Alloys: A Key Chemical Technology for Advanced Device Applications. *Coord. Chem. Rev.* **2013**, *257*, 2120−2141.

(4) Zhang, H.; Li, Y.; Tang, Q.; Liu, L.; Zhou, Z. First-Principles Studies on Structural and Electronic Properties of GaN−AlN Heterostructure Nanowires. *Nanoscale* **2012**, *4*, 1078−1084.

(5) Zhang, H.; Wu, D.; Tang, Q.; Liu, L.; Zhou, Z. ZnO-GaN Heterostructured Nanosheets for Solar Energy Harvesting: Computational Studies Based on Hybrid Density Functional Theory. *J. Mater. Chem. A* **2013**, *1*, 2231−2237.

(6) Geim, A. K.; Grigorieva, I. V. van der Waals Heterostructures. *Nature* **2013**, *499*, 419−425.

(7) Ponomarenko, L. A.; Geim, A. K.; Zhukov, A. A.; Jalil, R.; Morozov, S. V.; Novoselov, K. S.; Grigorieva, I. V.; Hill, E. H.; Cheianov, V. V.; Fal'ko, V. I.; Watanabe, K.; Taniguchi, T.; Gorbachev, R. V. Tunable Metal-Insulator Transition in Double-Layer Graphene Heterostructures. *Nat. Phys.* **2011**, *7*, 958−961.

(8) Yankowitz, M.; Xue, J.; Cormode, D.; Sanchez-Yamagishi, J. D.; Watanabe, K.; Taniguchi, T.; Jarillo-Herrero, P.; Jacquod, P.; LeRoy, B. J. Emergence of Superlattice Dirac Points in Graphene on Hexagonal Boron Nitride. *Nat. Phys.* **2012**, *8*, 382−386.

(9) Britnell, L.; Gorbachev, R. V.; Jalil, R.; Belle, B. D.; Schedin, F.; Mishchenko, A.; Georgiou, T.; Katsnelson, M. I.; Eaves, L.; Morozov, S. V.; Peres, N. M. R.; Leist, J.; Geim, A. K.; Novoselov, K. S.; Ponomarenko, L. A. Field-Effect Tunneling Transistor Based on Vertical Graphene Heterostructures. *Science* **2012**, *335*, 947−950.

(10) Dean, C.; Young, A. F.; Wang, L.; Meric, I.; Lee, G. H.; Watanabe, K.; Taniguchi, T.; Shepard, K.; Kim, P.; Hone, J. Graphene Based Heterostructures. *Solid State Commun.* **2012**, *152*, 1275−1282.

(11) Georgiou, T.; Jalil, R.; Belle, B. D.; Britnell, L.; Gorbachev, R. V.; Morozov, S. V.; Kim, Y.-J.; Gholinia, A.; Haigh, S. J.; Makarovsky, O.; Eaves, L.; Ponomarenko, L. A.; Geim, A. K.; Novoselov, K. S.; Mishchenko, A. Vertical Field-Effect Transistor Based on Graphene-WS_2 Heterostructures for Flexible and Transparent Electronics. *Nat. Nanotechnol.* **2012**, *8*, 100−103.

(12) Giovannetti, G.; Khomyakov, P. A.; Brocks, G.; Kelly, P. J.; van den Brink, J. Substrate-Induced Band Gap in Graphene on Hexagonal Boron Nitride: Ab initio Density Functional Calculations. *Phys. Rev. B* **2007**, *76*, 073103.

(13) Sławińska, J.; Zasada, I.; Klusek, Z. Energy Gap Tuning in Graphene on Hexagonal Boron Nitride Bilayer System. *Phys. Rev. B* **2010**, *81*, 155433.

(14) Ramasubramaniam, A.; Naveh, D.; Towe, E. Tunable Band Gaps in Bilayer Graphene−BN Heterostructures. *Nano Lett.* **2011**, *11*, 1070−1075.

(15) Ma, Y. D.; Dai, Y.; Guo, M.; Niu, C. W.; Huang, B. B. Graphene Adhesion on MoS_2 Monolayer: An ab initio Study. *Nanoscale* **2011**, *3*, 3883−3887.

(16) Du, A.; Sanvito, S.; Li, Z.; Wang, D.; Jiao, Y.; Liao, T.; Sun, Q.; Ng, Y. H.; Zhu, Z.; Amal, R.; Smith, S. C. Hybrid Graphene and Graphitic Carbon Nitride Nanocomposite: Gap Opening, Electron-Hole Puddle, Interfacial Charge Transfer, and Enhanced Visible Light Response. *J. Am. Chem. Soc.* **2012**, *134*, 4393−4397.

(17) Xu, P. T.; Tang, Q.; Zhou, Z. Structural and Electronic Properties of Graphene-ZnO Interfaces: Dispersion-Corrected Density Functional Theory Investigations. *Nanotechnology* **2013**, *24*, 305401.

(18) Kośmider, K.; Fernández-Rossier, J. Electronic Properties of the MoS_2-WS_2 Heterojunction. *Phys. Rev. B* **2013**, *87*, 075451.

(19) Terrones, H.; López-Urías, F.; Terrones, M. Novel Hetero-Layered Materials with Tunable Direct Band Gaps by Sandwiching Different Metal Disulfides and Diselenides. *Sci. Rep.* **2013**, *3*, 1549.

(20) Gan, L.-Y.; Zhao, Y.-J.; Huang, D.; Schwingenschlögl, U. First-Principles Analysis of MoS_2/Ti_2C and MoS_2/Ti_2CY_2 (Y = F and OH) All-2D Semiconductor/Metal Contacts. *Phys. Rev. B* **2013**, *87*, 245307.

(21) Komsa, H.; Krasheninnikov, A. V. Electronic structures and optical properties of realistic transition metal dichalcogenide heterostructures from first principles. *Phys. Rev. B* **2013**, *88*, 085318.

(22) Lu, N.; Guo, H.; Li, L.; Dai, J.; Wang, L.; Mei, W.; Wu, X.; Zeng, X. C. MoS_2/MX_2 heterobilayers: Bandgap engineering *via* tensile strain or external electrical field. *Nanoscale* **2014**, *6*, 2879−2886.

(23) Mak, K. F.; Lee, C.; Hone, J.; Shan, J.; Heinz, T. F. Atomically Thin MoS_2: A New Direct-Gap Semiconductor. *Phys. Rev. Lett.* **2010**, *105*, 136805.

(24) Gutiérrez, H. R.; Perea-López, N.; Elías, A. L.; Berkdemir, A.; Wang, B.; Lv, R.; López-Urías, F.; Crespi, V. H.; Terrones, H.; Terrones, M. Extraordinary Room-Temperature Photoluminescence in Triangular WS_2 Monolayers. *Nano Lett.* **2013**, *13*, 3447−3454.

(25) Tongay, S.; Zhou, J.; Ataca, C.; Lo, K.; Matthews, T. S.; Li, J.; Grossman, J. C.; Wu, J. Thermally Driven Crossover from Indirect toward Direct Bandgap in 2D Semiconductors: $MoSe_2$ versus MoS_2. *Nano Lett.* **2012**, *12*, 5576−5580.

(26) Sahin, H.; Tongay, S.; Horzum, S.; Fan, W.; Zhou, J.; Li, J.; Wu, J.; Peeters, F. M. Anomalous Raman Spectra and Thickness-Dependent Electronic Properties of WSe_2. *Phys. Rev. B* **2013**, *87*, 165409.

(27) (a) Li, Y.; Wu, D.; Zhou, Z.; Cabrera, C. R.; Chen, Z. Enhanced Li Adsorption and Diffusion on MoS_2 Zigzag Nanoribbons by Edge Effects: A Computational Study. *J. Phys. Chem. Lett.* **2012**, *3*, 2221−2227. (b) Jing, Y.; Zhou, Z.; Cabrera, C. R.; Chen, Z. F. Metallic VS_2 Monolayer: A Promising 2D Anode Material for Lithium Ion Batteries. *J. Phys. Chem. C* **2013**, *117*, 25409−25413.

(28) Radisavljevic, B.; Radenovic, A.; Brivio, J.; Giacometti, V.; Kis, A. Single-Layer MoS_2 Transistors. *Nat. Nanotechnol.* **2011**, *6*, 147−150.

(29) Lembke, D.; Kis, A. Breakdown of High-Performance Monolayer MoS_2 Transistors. *ACS Nano* **2012**, *6*, 10070−10075.

(30) Perkins, F. K.; Friedman, A. L.; Cobas, E.; Campbell, P. M.; Jernigan, G. G.; Jonker, B. T. Chemical Vapor Sensing with Monolayer MoS_2. *Nano Lett.* **2013**, *13*, 668−673.

(31) Li, Y.; Zhou, Z.; Zhang, S.; Chen, Z. MoS_2 Nanoribbons: High Stability and Unusual Electronic and Magnetic Properties. *J. Am. Chem. Soc.* **2008**, *130*, 16739−16744.

(32) Naguib, M.; Kurtoglu, M.; Presser, V.; Lu, J.; Niu, J. J.; Heon, M.; Hultman, L.; Gogotsi, Y.; Barsoum, M. W. Two-Dimensional

Nanocrystals Produced by Exfoliation of Ti_3AlC_2. *Adv. Mater.* **2011**, *23*, 4248−4253.
(33) Naguib, M.; Mashtalir, O.; Carle, J.; Presser, V.; Lu, J.; Hultman, L.; Gogotsi, Y.; Barsoum, M. W. Two-Dimensional Transition Metal Carbides. *ACS Nano* **2012**, *6*, 1322−1331.
(34) Khazaei, M.; Arai, M.; Sasaki, T.; Chung, C. Y.; Venkataramanan, N. S.; Estili, M.; Sakka, Y.; Kawazoe, Y. Novel Electronic and Magnetic Properties of Two-Dimensional Transition Metal Carbides and Nitrides. *Adv. Funct. Mater.* **2013**, *23*, 2185−2192.
(35) Lukatskaya, M. R.; Mashtalir, O.; Ren, C. E.; Dall'Agnese, Y.; Rozier, P.; Taberna, P. L.; Naguib, M.; Simon, P.; Barsoum, M. W.; Gogotsi, Y. Cation Intercalation and High Volumetric Capacitance of Two-Dimensional Titanium Carbide. *Science* **2013**, *341*, 1502−1505.
(36) Tang, Q.; Zhou, Z.; Shen, P. Are MXenes Promising Anode Materials for Li Ion Batteries? Computational Studies on Electronic Properties and Li Storage Capability of Ti_3C_2 and $Ti_3C_2X_2$ (X = F, OH) Monolayer. *J. Am. Chem. Soc.* **2012**, *134*, 16909−16916.
(37) (a) Naguib, M.; Halim, J.; Lu, J.; Cook, K. M.; Hultman, L.; Gogotsi, Y.; Barsoum, M. W. New Two-Dimensional Niobium and Vanadium Carbides as Promising Materials for Li-Ion Batteries. *J. Am. Chem. Soc.* **2013**, *135*, 15966−15969. (b) Xie, X. H.; Chen, S. G.; Ding, W.; Nie, Y.; Wei, Z. D. An Extraordinarily Stable Catalyst: Pt NPs Supported on Two-Dimensional $Ti_3C_2X_2$ (X = OH, F) Nanosheets for Oxygen Reduction Reaction. *Chem. Commun.* **2013**, *49*, 10112−10114. (c) Gan, L.-Y.; Huang, D.; Schwingenschloegl, U. Oxygen Adsorption and Dissociation During the Oxidation of Monolayer Ti_2C. *J. Mater. Chem. A* **2013**, *1*, 13672−13678.
(38) Chen, Y.; Xi, J.; Dumcenco, D. O.; Liu, Z.; Suenaga, K.; Wang, D.; Shuai, Z.; Huang, Y.-S.; Xie, L. Tunable Band Gap Photoluminescence from Atomically Thin Transition-Metal Dichalcogenide Alloys. *ACS Nano* **2013**, *7*, 4610−4616.
(39) Hwu, S. J.; Ziebarth, R. P.; Winbush, S. V.; Ford, J. E.; Corbett, J. D. Synthesis and Structure of Double-Metal-Layered Scandium, Yttrium, and Zirconium Chloride Carbides and Nitrides, $M_2C_{12}C$ and $M_2C_{12}N$. *Inorg. Chem.* **1986**, *25*, 283−287.
(40) Segall, M. D.; Lindan, P. J. D.; Probert, M. J.; Pickard, C. J.; Hasnip, P. J.; Clark, S. J.; Payne, M. C. First-Principles Simulation: Ideas, Illustrations and the CASTEP Code. *J. Phys.: Condens. Matter* **2002**, *14*, 2717−2744.
(41) Perdew, J. P.; Wang, Y. Accurate and Simple Analytic Representation of the Electron-Gas Correlation Energy. *Phys. Rev. B* **1992**, *45*, 13244−13249.
(42) Ortmann, F.; Bechstedt, F.; Schmidt, W. G. Semiempirical van der Waals Correction to the Density Functional Description of Solids and Molecular Structures. *Phys. Rev. B* **2006**, *73*, 205101.
(43) Heyd, J.; Scuseria, G. E.; Ernzerhof, M. Hybrid Functionals Based on a Screened Coulomb Potential. *J. Chem. Phys.* **2003**, *118*, 8207−8215.